2023 IEEE/ASME International Conference on Advanced Intelligent Mechatronics (AIM)
June 28-30, 2023. Seattle, Washington, USA

Independent Tendons Increase Stiffness of Continuum Robots without Actuator Coupling

Parsa Molaei, Nekita A. Pitts, and Hunter B. Gilbert
Mechanical and Industrial Engineering
Louisiana State University
Baton Rouge, Louisiana, USA
pmolae1@lsu.edu, npitts2@lsu.edu, hbgilbert@lsu.edu

***Abstract*—Tendon-driven continuum robots have drawn interest for a wide variety of applications. Prior work in this area has elucidated the coupled kinematics and statics models that describe the motion and coupling of the robot's elastic backbone with the driving tendons that are tensioned to change the shape of the robot. However, the full design freedom associated with the routing of the tendon through the supporting "eyelets" in the structure has not been explored. This article describes designs that have multiple tendon paths designed to influence the shape of only one continuously deformable section. It is known that this type of solution generally results in highly coupled tendon kinematics, but we show experimentally that there exist paths for which the tendons are so weakly coupled (kinematically) that they can be locked off to provide configuration-independent stiffening. They could also be displaced independently from one another to control independent deformation modes. The approach reveals a strategy for reducing the uncontrolled compliance of the robot's body, including the torsional compliance, while retaining simplicity in design and control. In particular, we show that tendons that are routed sinusoidally and helically do not strongly couple to constant-curvature actuating tendons as long as they meet an orthogonality constraint. The added tendons increase the stiffness at the cantilevered end by 4.85x over straight tendons alone without impacting the range of motion in the stiffened condition.**

***Index Terms*—Tendon/wire mechanism, flexible robots, continuum robots, compliant joint mechanism**

Fig. 1. A tendon-driven continuum robot prototype, consisting of a flexible backbone and several sets of tendons routed through guides over the length of the flexible section.

I. Introduction

A. Background

Tendon-driven robots and other high-DOF tendon-driven structures have been investigated for a vast range of applications, including minimally invasive surgery [1], [2], space manipulators [3], [4], nuclear inspection [5], and as general purpose robots for grasping and manipulation in unstructured environments [6]. A tendon-driven continuum robot consists of a flexible elastic member that supports multiple tendon-guides and tendons which are used to pull on the guides to deform the structure (Fig. 1) [7]. These robots have many similar properties to underactuated hyperredundant robots, such as the need to provide internal forces to resolve the configuration of the robot and the need for models to couple kinematics and statics or dynamics.

The flexible backbone provides some advantages for the soft robot compared to the traditional manipulators with multiple physical joints, and it may provide advantages in highly congested environments [8]. The elastic compliance may allow the robot to respond favorably to the environment, and remotely tendon-actuated structures can often be made compact and lightweight in space- and mass-constrained applications. In such cases, the elastic compliance is either necessary to secure interactions with the unpredictable environment and to safeguard both the robot and its workspace or it is simply a byproduct of highly slender robot arm designs for applications like minimally invasive surgery [9].

A well-designed continuum robot should take full advantage of its structural properties to achieve a desirable level of versatility, control, accessibility, dependability, and perhaps most importantly, structural stability. An effort to find technologies and approaches to strike the balance between "too stiff" and "too soft" has ensued for both rigid-link manipulators and continuum or hyperredundant manipulators, with tunable stiffness being seen generally as advantageous [10]. One specific use for variable stiffness structures is to enable navigation through tortuous spaces [11].

*Corresponding Author
This work was supported in part by funding from the National Science Foundation under Grant Number 2133019 and in part by the Louisiana Space Grant Consortium under NASA Grant Number 80NSSC20M0110 and Louisiana Board of Regents Grant Number LEQSF(2020-2024)-LaSPACE.

Many methods have been studied to achieve a desirable manipulator stiffness–usually this means an increase in stiffness for continuum robots–such as granular jamming and fiber jamming. Both of these technologies can be turned on and off through the application or removal of a vacuum, enabling a reversible change in stiffness [12], [13]. There are also other forms of locking using friction, mechanical interference, and phase changing materials such as Field's metal and shape memory alloys [14], [15]. Some approaches to enabling the control of more degrees of freedom, such as shape-locking mechanisms, also affect stiffness [16]. However, in general, these approaches all have a similar drawback if only a change in stiffness is desired: the change in stiffness is the result of a change in the mechanical properties of the elastic body, which affects the response to actuation (i.e., the internal loads) as well as the response to external loads.

It is known that a typical tendon-driven continuum manipulator have different relative stiffness to external loads at different locations on the body depending on what modes of deformation are being actuated by the included tendons. It is known that tendon paths which converge or diverge from the elastic backbone result in significant changes in the distribution of stiffness when compared to typical straight tendon paths, and the behavior under prescribed tendon tension (low tendon stiffness), is fundamentally different from the behavior under prescribed tendon displacement (high tendon stiffness), and that the stiffness of the tendon-driven robot cannot be increased via increasing the pretension. Increasing the pretension could result in the increase of static frictional forces on the tendons which could indirectly affect the stiffness. [17]. In addition, tendon paths that cross over the backbone which create "S" shape tendon guides in continuum robots have been used as a decoupling strategy in continuum robots, and that utilizing different tendon routing approaches can decrease the tendon coupling between individual joints in multi-joint continuum robots [18]. A novel design strategy was introduced by implementing new assumptions into prior modeling approaches [19], [20] to compensate for the results of the unwanted modes of deformation and to enhance the control of the shape and stiffness of the tendon-driven continuum manipulator.

B. Contributions

In this paper, we extend our recently published results in Molaei et al. [21] and expand the ideas to include new tendon routing options, including tendons that are routed simultaneously in a helical configuration and multiple cosine shapes. We describe the design of a prototype used to validate the predicted modeling approach in Section 3. Section 4 presents the results of a kinematic simulation and experimental evaluation of the design. Section 5 compares and discusses the results from the experiments and the simulations and offers concluding remarks and ideas for future research directions.

II. Modeling

We modeled the robot using a constant curvature kinematic simulation, treating the tendon supports as rigid bodies located in the normal cross sections to the elastic backbone. The constant curvature method assumes that the shape of the backbone after deformation is that of a circle having curvature κ in units of radians per meter. Over varying curvatures, the simulation calculates the point-to-point distance between the tendon supports and sums these distances to find the total length of the tendon. The basic modeling approach is rooted in the idea of constant curvature kinematics and a partially supported tendon path [20], [22].

To describe the method briefly, we assume that the initial undeformed shape is straight and that the backbone lies along the y-axis of the simulation coordinate system, with the base of the robot at the origin. We assume that the shape is described by a circular arc in the $y - z$ plane, i.e. the curvature is described by the axial vector $\kappa = \begin{bmatrix}\kappa_x & 0 & 0\end{bmatrix}^T$ We use the "hat" notation to denote the standard coordinate mapping from $\mathbb{R}^6$ to $\mathfrak{se}(3)$, $\exp : \mathfrak{se}(3) \to SE(3)$ the exponential mapping, e_2 the 2nd standard basis vector for $\mathbb{R}^3$, and y_i the undeformed y-coordinate to the location of the ith tendon support disk. Then, the ith coordinate transformation associated with the ith tendon support disk is given by

$$T_i^0 = \exp(y_i\hat{\xi}) \qquad \xi = \begin{bmatrix} e_2 \\ \kappa \end{bmatrix} \tag{1}$$

In coordinate frame $\mathcal{F}_i$ associated with the ith tendon support disk, the coordinates of the tendon support locations are fixed as indicated in 2 and Table II. Then, finally, the length of the tendon which passes through support holes with positions $r_{i,j}$, the first index being the number of the tendon and the second being the sequential hole index for that tendon, is modeled by

$$L_i = \sum_{j=1}^{N} \| T_{j+1}^0(r_{i,j+1}) - T_j^0(r_{i,j}) \| \tag{2}$$

In using this length function, it is implicitly assumed that all tendons remain taut during a displacement.

Unlike a partially supported tendon, a fully supported tendon is instead described by a functional form with respect to the length along the axial coordinate of the robot: $r_i(s) = r_{ix}(s)x(s) + r_{iz}(s)z(s)$. In this case, the arc length coordinate s describes the position along the backbone, and vectors $x(s)$ and $z(s)$ are orthogonal unit vectors spanning the cross-section normal to the backbone. Then, the two functions $r_{ix}(s)$ and $r_{iz}(s)$ describe the location of the tendon. In our prior work [21] we showed in the planar case that a design condition exists that can decouple the tendon lengths to the first order with respect to changes in the curvature of the backbone. A relatively straightforward extension to the spatial case led to

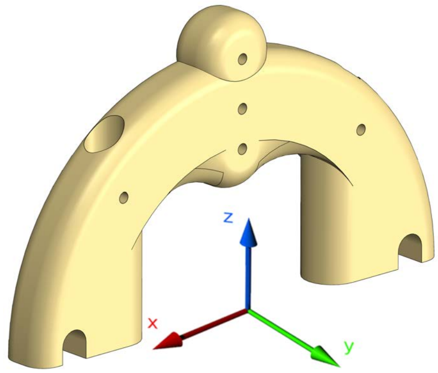

Fig. 2. Coordinate system describing the relative coordinates of the tendon support positions.

the hypothesis that the following fully supported tendon paths would all be decoupled:

$$\begin{aligned} r_1(s) &= a_1 z(s) \\ r_2(s) &= a_2 \cos(\pi/L) z(s) \\ r_3(s) &= a_3 \cos(3\pi/L) z(s) \\ r_4(s) &= a_4 \left(\cos(3\pi/L) z(s) + \sin(3\pi/L) x(s)\right) \end{aligned} \tag{3}$$

The tendon paths chosen in this work are the partially supported approximations developed by sampling these continuous functions at discrete arc lengths s_j.

III. Experimental Validation

A. Prototype Design

The construction of the model robot involved the use of a lightweight composite material, a 2-ply carbon fiber/epoxy laminate, to serve as the backbone of the robot. The resin infused CF laminate used in the construction had a thickness of 0.59mm and was made from a 3K weave pattern fabric (Composite Envisions, Wausau, WI, USA). 13 individual tendon support structures were manufactured and printed using an SLA 3D printer (Photon M3, Anycubic, HongKong) with standard 405 nm UV wave length resin. The robot's dimensions are described in Table I and shown in Fig. 3. The tendon support placements and eyelet positions on the tendon support disks for the C_1, C_2, and H tendons are described in Table II while the Actuating tendons have a constant distant of 30 mm from the backbone. A smooth braided fishing line with 10 lbs of break strength was selected for tendons of the robot prototype (Stealth Smooth 8, 10lb, SpiderWire, CA, USA). One end of the tendons were knotted to the base end of the robot and fixed and the other end of the tendons were connected to the adjustable tendon tensioners that were designed and 3D printed for the free end of the robot. The tendon tensioners include 4 individual worm and worm wheel mechanisms to adjust the tendon tensions independently from one another. Because our only present aim is to study the mechanics of the structure, motors and controllers are not needed and were not included.

TABLE I
Prototype robot design parameters.

Parameter	Symbol	Value
Backbone length	L	270 mm
Backbone height	h	60 mm
Backbone thickness	t	0.59 mm
No. of tendon supports	N	13
tendon support spacing	ΔL	22.5 mm

TABLE II
Prototype tendon support locations and radii.

		C_1		C_2		H	
Index, i	y (mm)	x (mm)	z (mm)	x (mm)	z (mm)	x (mm)	z (mm)
0	0	0	25.0	0	25.0	0	25.0
1	22.5	0	24.1	0	19.4	17.7	17.7
2	45.0	0	21.6	0	0	25.0	0
3	67.5	0	17.6	0	-19.4	17.7	-17.7
4	90.0	0	12.5	0	-25.0	0	-25.0
5	112.5	0	6.4	0	-19.4	-17.7	-17.7
6	135.0	0	0	0	0	-25.0	0
7	157.5	0	-6.4	0	19.4	-17.7	17.7
8	180.0	0	-12.5	0	25.0	0	25.0
9	202.5	0	-17.6	0	19.4	17.7	17.7
10	225.0	0	-21.6	0	0	25.0	0
11	247.5	0	-24.1	0	-19.4	17.7	-17.7
12	270.0	0	-25.0	0	-25.0	0	-25.0

B. Characterization under a distributed gravity load

After the initial assembly of the robot, without any tendons pre-tensioned, the robot was positioned horizontally with the flexible direction of the beam oriented with gravity so that the distributed gravity load of the support disks and the tensioning assembly tend to deflect the body of the robot, and a photograph was taken. Then, the actuating tendon pair is first pre-tensioned so that when the stiff direction of the backbone is turned against gravity, the beam is straight. After again orienting the robot so that the flexible direction is aligned with gravity, another photograph was taken. Then, subsequent tendons are pre-tensioned such that the backbone remains as straight as possible by visual inspection, with photographs taken at each stage of the assembly to assess the impact of the additional tendons on shape-retention without any external point loads.

C. Characterization under point loads

An industrial robot manipulator (UR5e, Universal Robots, Odense, Denmark) was used to push the robot's backbone at different locations and the reaction forces caused by the implied motion was recorded using a high precision beam load cell (LSP-5, range: 0–5N, Transducer Techniques, Temecula, CA, USA). The load cell was attached to the end effector of the UR5e robot using a custom made 3D printed bracket. A push block attachment was 3D printed to provide contact structure for the free end of the load cell. A commercial load cell amplifier is used to power the load cell bridge and condition the

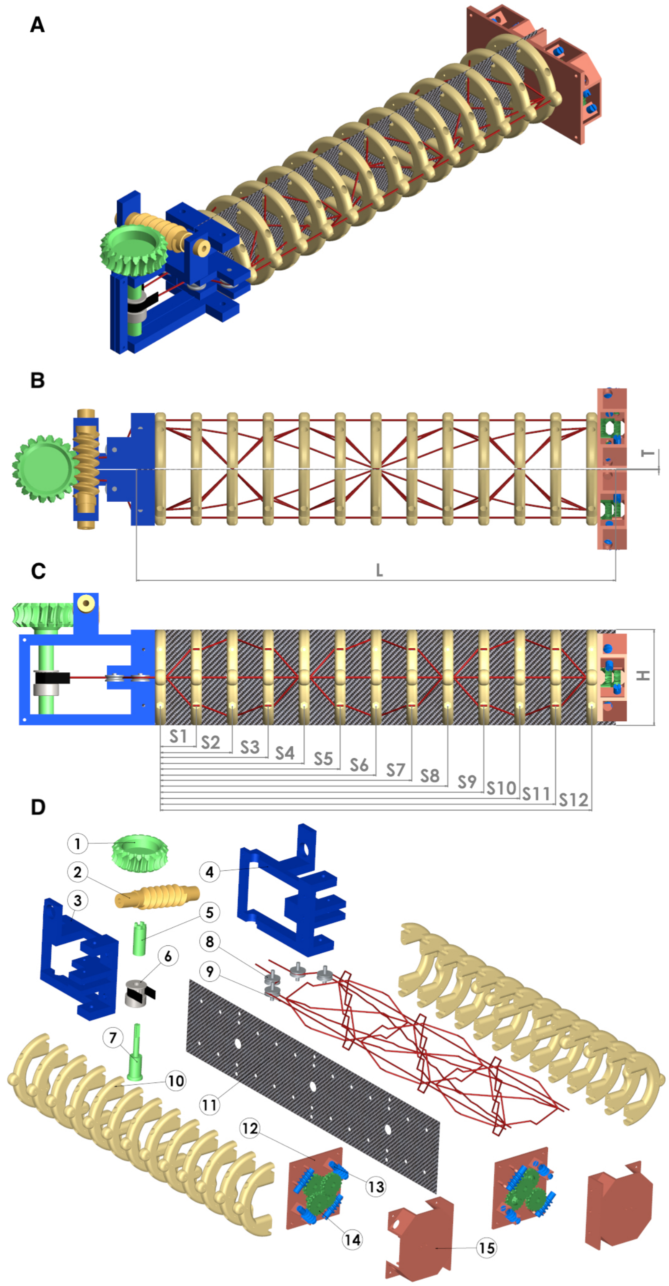

Fig. 3. A. Isometric view (assembled). B. Top view (assembled). C. Side view (assembled). D. Exploded view. ① Worm gear ② Worm ③ Base frame - right ④ Base frame - left ⑤ Supporting shaft ⑥ timing pulley and belt ⑦ Supporting shaft - lower ⑧ tendon routing pulley ⑨ tendons ⑩ tendon supports ⑪ Backbone ⑫ Tensioner housing ⑬ Tensioner worm ⑭ Tensioner gear ⑮ Tensioner clamp

output signal (LCA-RTC, Transducer Techniques, Temecula, CA, USA). The output of the amplifier is digitized by a USB DAQ (USB-1808X, Measurement Computing, Norton, MA, USA). The complete experimental setup is shown in the Fig. 4.

The UR5e robot was set to produce a controlled motion with constant speed and the complete motion of the end effector was recorded and monitored using 3D motion capture cameras (Flex13, 4 cameras, OptiTrack, City, State, USA). A support structure was designed and built for the tendon-driven robot to attach and be placed in front of the UR5e manipulator. The UR5e robot was set to exert force by applying controlled displacements on each of the tendon support disks of the tendon-driven continuum robot. Both the motion of the supports and the analog voltage samples from the load cell amplifier were recorded at 30 S/s. The maximum displacement of each tendon support disk was adjusted individually to ensure that the forces were within the sensing range of the load cell. Each test was run three different times to calculate uncertainties. After collecting the data from the load cell and the motion detecting camera system, a coordinate transform was performed to align the recorded motion of the UR5e end-effector with our defined coordinate directions. The peak values for the displacement and force measurements were extracted manually and a linear model (4) was fit to 400 samples before and after each peak to produce a force vs. displacement response.

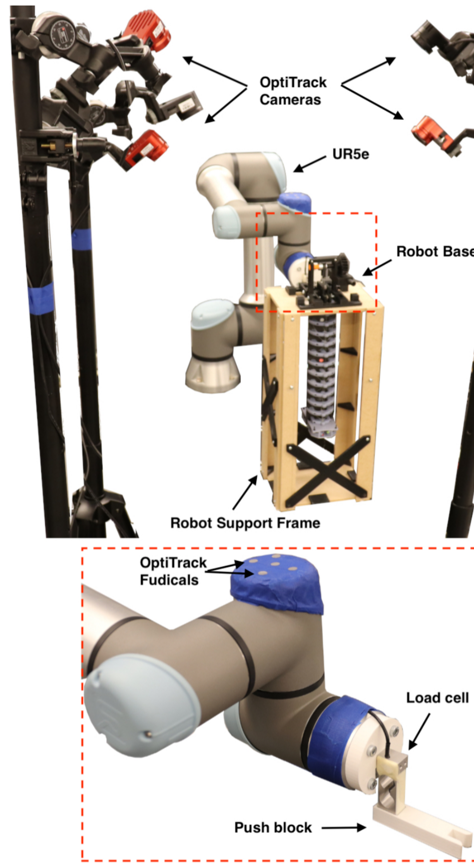

Fig. 4. Experimental setup for stiffness characterization of the tendon-driven continuum robot for contact forces applied at different locations along the robot.

$$F_{\mathrm{kl}} = \beta_{\mathrm{k}} X + \eta_{\mathrm{kl}} \tag{4}$$

The index k = 3, . . . , 13 indicates the contact location and the index l = 1, 2, 3 indicates the experimental repetition. β_k are the stiffnesses observed at each contact location, x is

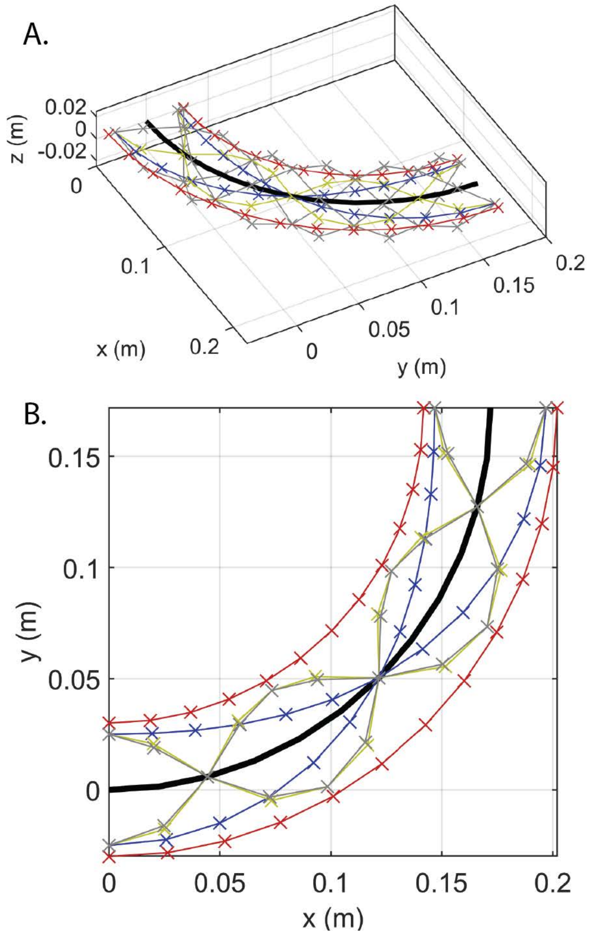

Fig. 5. Graphical depiction of the kinematic simulation results, showing the elastic backbone (dark, thick line) along with the tendons. Crosses indicate the tendon support locations.

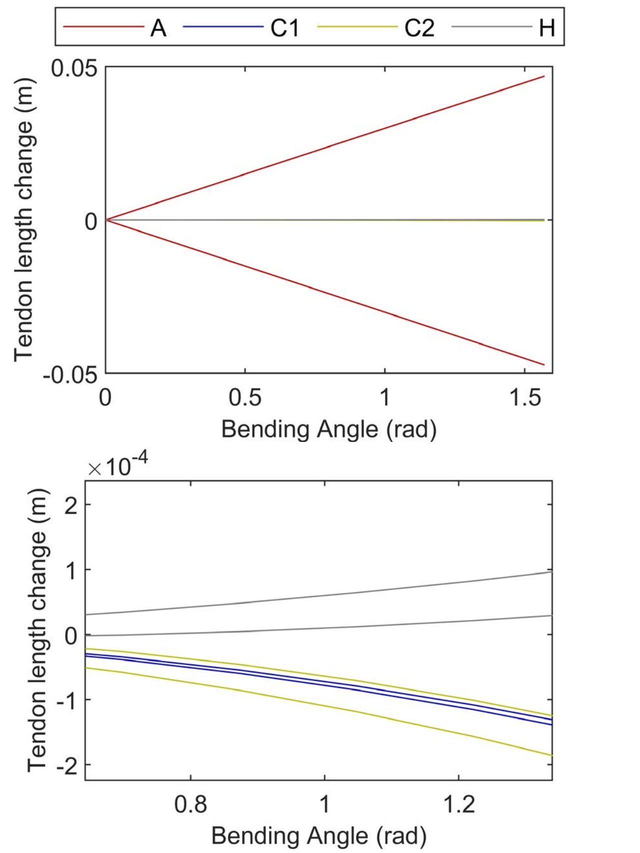

Fig. 6. (Top) Tendon length changes as a function of constant curvature bending angle. It is clearly seen that over 90 degrees of bending, only the actuating tendons have a significant change in path length. (Bottom) Zoomed-in view. The stiffening tendon paths C1, C2, and H have less than two-tenths of a millimeter change in length for the robot with the described dimensions.

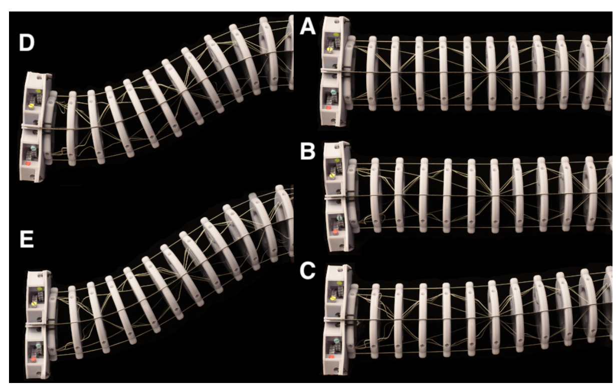

Fig. 7. Observable stiffness of the robot under different initial pre-tension loads of the stiffening tendons. Ⓐ: State AC_1C_2H Ⓑ: State AC_1C_2 Ⓒ: State AC_1 Ⓓ: State AC_2 Ⓔ: State A.

the rotated end-effector coordinate of the UR5, and η_{kl} is a contact-location and repetition-dependent bias term.

IV. Results

A. Kinematic Simulations

Simulation results following the piecewise constant curvature method [22] based on the design parameters of the prototype robot are shown in Fig. 5 and 6. Between 0 and 90 degrees of bending, the simulations predict a total path length change of no more than 0.2 mm for any of the stiffening tendons. The results from the kinematic simulations demonstrate that the tendon decoupling for the chosen tendon path C_1, C_2, and H is acceptable and the amount of length change is negligible. Given a small amount of stretch in the tendons themselves and a small amount of flexibility in the tie-off points of the tendons, it may be expected with good certainty that they will remain taut. If it were desired that these tendons maintain an approximately constant pretension during the motion, further analysis and design might be required, which was not performed.

B. Characterization under distributed gravity load

The results of the gravity load characterization are shown in Fig. 7. It is seen clearly that the additional tendons substantially reduce the effect of the self-weight of the robot. With only straight actuating tendons, the load tends to produce a sigmoid-shaped curve in the backbone, which is a result of the

TABLE III

STIFFNESS MULTIPLE AT EACH TENDON SUPPORT DISK RELATIVE TO STATE A

	Disk 3	Disk 4	Disk 5	Disk 6	Disk 7	Disk 8	Disk 9	Disk 10	Disk 11	Disk 12	Disk 13
State AC_1C_2H	2.63	3.58	3.35	3.85	4.29	5.78	5.76	6.49 *	5.58	5.52	4.85
State AC_1H	2.61	3.03	2.92	3.27	3.64	4.39	5.05	5.40 *	4.54	4.69	4.19
State AC_1C_2	1.98	2.63	2.49	2.71	3.45	4.10	4.65	5.54 *	4.41	4.29	3.77
State AC_1	1.84	2.44	2.61	2.71	3.19	3.53	4.29	5.20 *	4.19	4.06	3.55
State AC_2H	2.43	2.43 *	2.00	1.71	1.69	1.68	1.59	1.49	1.37	1.50	1.49
State AH	2.30 *	2.04	1.60	1.41	1.38	1.41	1.31	1.33	1.14	1.24	1.15
State AC_2	2.00 *	1.02	1.05	1.12	1.27	1.21	1.14	1.20	1.03	1.11	1.15
State A	1.00	1.00	1.00	1.00	1.00	1.00	1.00	1.00	1.00	1.00	1.00
State N	0.96 *	0.92	0.92	0.88	0.85	0.76	0.73	0.68	0.57	0.60	0.50

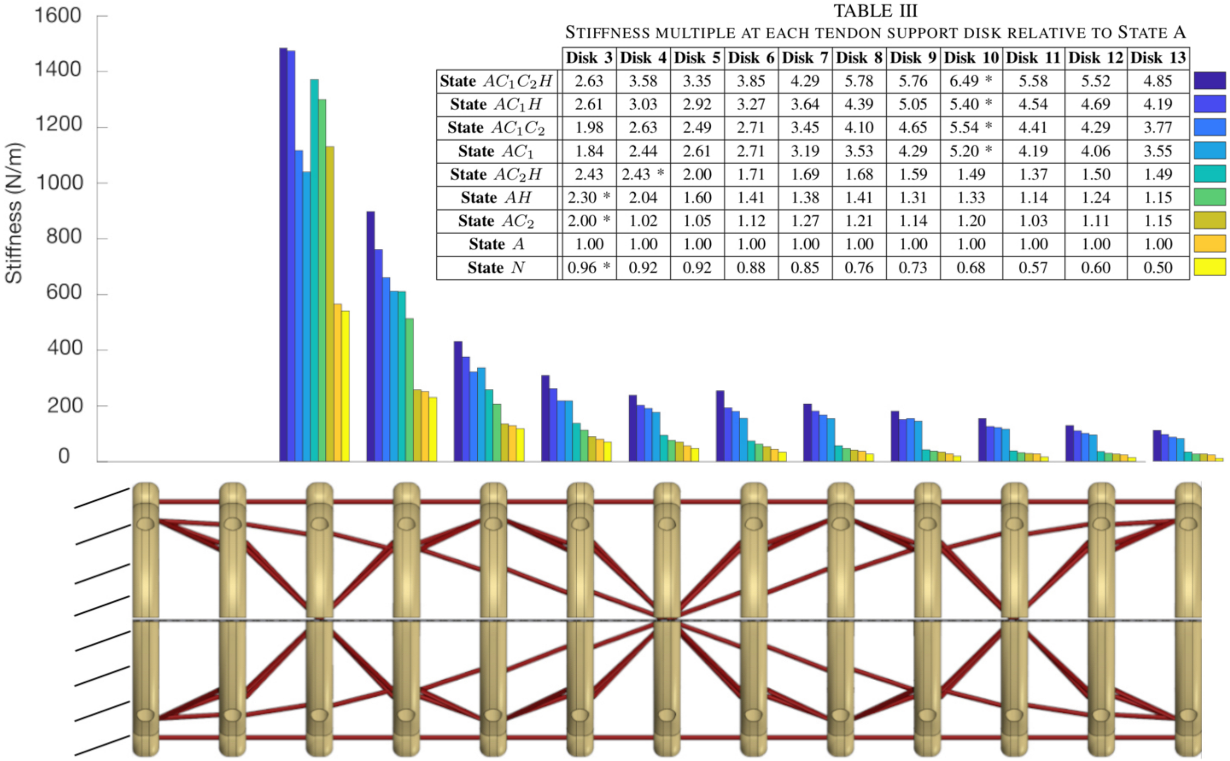

Fig. 8. Stiffness along the length of the tendon-driven robot with one fixed boundary condition. Bars indicate stiffness and are grouped by physical location of the measurement (at each of the tendon support structures). Stiffness is measured across the factor of condition of tendon pre-tensioning with the factors being (N) no tendons pre-tensioned, (A) actuating tendons only pre-tensioned, (AC2) Actuating and second cosine stiffening tendons pre-tensioned, (AH) Actuating and helical tendons pre-tensioned, (AC2H) Actuating, second cosine stiffening tendons and helical tendons pre-tensioned, (AC1) Actuating, and first cosine stiffening tendons pre-tensioned, (AC1C2) Actuating, first and second cosine stiffening tendons pre-tensioned, (AC1H) Actuating, first cosine stiffening tendons and helical tendons pre-tensioned, (AC1C2H) Actuating, first and second cosine stiffening tendons, and helical tendons pre-tensioned.

fact that this shape does not substantially change the length of the straight tendon paths (the tendon spends approximately equal length on the positive and negative curvature side of the backbone).

C. Characterization under point loads

Following the linear regression that was introduced in the (4), stiffness values of β_k were extracted for each tendon pre-tensioning State at 11 different tendon path support disks along the length of the robot. Fig. 8 shows the result graphically, and Table III reports the percentage increases in stiffness relative to the cantilevered state with no tendons. It is clearly observed that at every disk, the state with all tendons is the stiffest. Values were not measured at the second support disk from the fixed base due to the stiffness being too high to reliably measure using our experimental setup. Recorded values for the stiffness measurements, β_k, for each one of the pre-tensioning states shows significant difference based on the combination of the tendons that are pre-tensioned. Since our previous work has already established that the stiffening tendons have a major impact only when combined with the actuating tendons, we did not investigate combinations lacking the actuating tendon, with the one exception of a control case having no tendons (a simple cantilever beam).

During the experiment, it was observed in some of the pre-tensioing states that the deflection response of the robot's backbone is not well modeled by a regular Euler-Bernoulli cantilever beam. Hence, an increase or decrease in the stiffness of the robot at a specific section of the beam compared to another pre-tensioning state would not mean that the stiffness measurements would follow the same trend in the other pre-tensioning state. In other words, adding pre-tension to an extra set of tendons does not guarantee an increase in the stiffness at every location along the length of the robot.

V. DISCUSSION

With the chosen prototype design parameters and the range of pre-tensions that were tested, for every State of pre-tension, an increase in pre-tension resulted in an increase in the observable stiffness at every tendon support location except for state AC_1C_2 and AC_1 where the added pre-tension to the C_2 tendon caused a decrease in the stiffness at the location of the support disk 5, and for state AC_1C_2 and AC_2 were the added pre-tension to the C_1 tendon caused a decrease in the stiffness at the location of the support disk 3. These decreases could be the result of compressive stress in the elastic backbone causing foreshortening work, an effect which is known to decrease transverse stiffness of beams [23]. It is also possible that nonlinear friction effects in the tendons could influence the stiffness measurements.

Although it was not measured due to limitations of the present experimental setup, by hand manipulation we observed a major difference in the torsional stiffness of the structure when the helical tendons are included among the pretensioned tendons. The ability to improve the torsional stiffness may have important effects, such as the potential elimination of lateral-torsional buckling instability when curved arch-like structures are subjected to in-plane loads [24].

The lack of coupling between the straight actuating tendons and the other stiffening tendons also implies that the stiffening tendons could be converted to independent actuating tendons that exercise control over independent shape modes. This approach would be an interesting alternative to the use of "multisection" designs which terminate tendons at multiple lengths, which causes a complex coupling of motions and forces between the sets of tendons [25], [26].

VI. Conclusion

We have presented a simple approach which enables large changes in structural stiffness (or, alternatively, actuation of independent mode shapes). This approach has the major benefit of negligible impact on the actuation of the robot. A prototype demonstrated a 4.85x increase in stiffness at the endpoint, with substantial improvement in torsional rigidity. Future work will explore the simultaneous actuation of multiple shape modes and quantify the impacts of this approach on the stability, stiffness distribution, and precision of load manipulation. In addition, the effects of the stiffening cables on the final resulting shape from the actuating cables will be explored to compare and evaluate that if introducing the stiffening cables has improved the ability of the actuating cables to achieve the desired and anticipated curvature mode by constraining the extra modes of deformation.

References

[1] D. Camarillo, C. Carlson, and J. Salisbury, "Configuration Tracking for Continuum Manipulators With Coupled Tendon Drive," *IEEE Trans. Robot.*, vol. 25, no. 4, pp. 798–808, 2009.

[2] M. S. Moses, R. J. Murphy, M. D. M. Kutzer, and M. Armand, "Modeling Cable and Guide Channel Interaction in a High-Strength Cable-Driven Continuum Manipulator," *IEEE/ASME Trans. Mechatronics*, vol. 20, no. 6, pp. 2876–2889, 2015.

[3] M. Mahlin, R. L. Wagner, J. Dorsey, and T. C. Jones, "Tendon-Actuated Lightweight In-Space MANipulator (TALISMAN) Hinge Joint Structural," in *ASCEND 2020*, 2020.

[4] J. Mehling, M. Diftler, M. Chu, and M. Valvo, "A minimally invasive tendril robot for in-space inspection," in *IEEE/RAS-EMBS Int. Conf. on Biomedical Robotics and Biomechatronics*, 2006, p. 690–695.

[5] R. Buckingham and A. Graham, "Nuclear snake-arm robots," *Industrial Robot: An International Journal*, vol. 39, no. 1, pp. 6–11, 2012.

[6] I. Walker and M. Hannan, "A novel "elephant's trunk" robot," in *IEEE/ASME Int. Conf. on Advanced Intelligent Mechatronics (Cat. No.99TH8399)*, 1999, p. 410–415.

[7] G. Robinson and J. B. C. Davies, "Continuum robots-a state of the art," in *IEEE Int. Conf. Robot. Autom.*, vol. 4, 1999, p. 2849–2854.

[8] D. Trivedi, C. D. Rahn, W. M. Kier, and I. D. Walker, "Soft robotics: Biological inspiration, state of the art, and future research," *Applied Bionics and Biomechanics*, vol. 5, no. 3, p. 99–117, 2008.

[9] J. Burgner-Kahrs, D. C. Rucker, and H. Choset, "Continuum robots for medical applications: A survey," *IEEE Trans. Robot.*, vol. 31, no. 6, p. 1261–1280, 2015.

[10] C. Laschi and M. Cianchetti, "Soft Robotics: New Perspectives for Robot Bodyware and Control," *Front. Bioengineering and Biotechnology*, vol. 2, 2014.

[11] A. Degani, H. Choset, A. Wolf, and M. Zenati, "Highly articulated robotic probe for minimally invasive surgery," in *IEEE Int. Conf. Robot. Autom.*, 2006, p. 4167–4172.

[12] M. Cianchetti, T. Ranzani, G. Gerboni, T. Nanayakkara, K. Althoefer, P. Dasgupta, and A. Menciassi, "Soft robotics technologies to address shortcomings in today's minimally invasive surgery: The stiff-flop approach," *Soft Robotics*, vol. 1, no. 2, p. 122–131, 2014.

[13] B. Aktas and R. D. Howe, "Tunable anisotropic stiffness with square fiber jamming," in *IEEE Int. Conf. on Soft Robotics*, New Haven, CT, USA, 2020, p. 879–884.

[14] F. Alambeigi, R. Seifabadi, and M. Armand, "A continuum manipulator with phase changing alloy," in *IEEE Int. Conf. Robot. Autom.*, 2016, p. 758–764.

[15] Y. Kim, S. S. Cheng, and J. P. Desai, "Active stiffness tuning of a spring-based continuum robot for mri-guided neurosurgery," *IEEE Trans. Robot.*, vol. 34, no. 1, p. 18–28, 2018.

[16] C. Pogue, P. Rao, Q. Peyron, J. Kim, J. Burgner-Kahrs, and E. Diller, "Multiple curvatures in a tendon-driven continuum robot using a novel magnetic locking mechanism," in *IEEE/RSJ Int. Conf. on Intell. Robots Syst.*, 2022, p. 472–479.

[17] K. Oliver-Butler, J. Till, and C. Rucker, "Continuum Robot Stiffness Under External Loads and Prescribed Tendon Displacements," *IEEE Trans. Robot.*, vol. 35, no. 2, pp. 403–419, 2019.

[18] Y. Chitalia, S. Jeong, N. Deaton, J. J. Chern, and J. P. Desai, "Design and Kinematics Analysis of a Robotic Pediatric Neuroendoscope Tool Body," *IEEE/ASME Trans. Mechatronics*, vol. 25, no. 2, pp. 985–995, 2020.

[19] D. C. Rucker and R. J. Webster III, "Statics and Dynamics of Continuum Robots With General Tendon Routing and External Loading," *IEEE Trans. Robot.*, vol. 27, no. 6, pp. 1033–1044, 2011.

[20] P. Rao, Q. Peyron, S. Lilge, and J. Burgner-Kahrs, "How to Model Tendon-Driven Continuum Robots and Benchmark Modelling Performance," *Front. Robotics and AI*, vol. 7, p. 630245, 2021.

[21] P. Molaei, N. A. Pitts, G. Palardy, J. Su, M. K. Mahlin, J. H. Neilan, and H. B. Gilbert, "Cable decoupling and cable-based stiffening of continuum robots," *IEEE Access*, vol. 10, p. 104852–104862, 2022.

[22] R. J. Webster and B. A. Jones, "Design and Kinematic Modeling of Constant Curvature Continuum Robots: A Review," *Int J Rob Res*, vol. 29, no. 13, pp. 1661–1683, 2010, publisher: SAGE Publications Ltd STM.

[23] J. Mayo, J. Dominguez, and A. A. Shabana, "Geometrically nonlinear formulations of beams in flexible multibody dynamics," *Journal of Vibration and Acoustics*, vol. 117, no. 4, p. 501–509, 1995.

[24] Y. L. Pi, M. A. Bradford, and G. S. Tong, "Elastic lateral–torsional buckling of circular arches subjected to a central concentrated load," *International Journal of Mechanical Sciences*, vol. 52, no. 6, p. 847–862, 2010.

[25] B. Jones and I. Walker, "Kinematics for multisection continuum robots," *IEEE Trans. Robot.*, vol. 22, no. 1, p. 43–55, 2006.

[26] P. S. Gonthina, M. B. Wooten, I. S. Godage, and I. D. Walker, "Mechanics for Tendon Actuated Multisection Continuum Arms," in *IEEE Int. Conf. on Robotics and Automation*, 2020, pp. 3896–3902.